

Differential Dynamic Programming Neural Optimizer

Guan-Horng Liu¹ Tianrong Chen¹ Evangelos A. Theodorou¹

Abstract

Interpretation of Deep Neural Networks (DNNs) training as an optimal control problem with non-linear dynamical systems has received considerable attention recently, yet the algorithmic development remains relatively limited. In this work, we make an attempt along this line by reformulating the training procedure from the trajectory optimization perspective. We first show that most widely-used algorithms for training DNNs can be linked to the Differential Dynamic Programming (DDP), a celebrated second-order trajectory optimization algorithm rooted in the Approximate Dynamic Programming. In this vein, we propose a new variant of DDP that can accept batch optimization for training feedforward networks, while integrating naturally with the recent progress in curvature approximation. The resulting algorithm features *layer-wise feedback policies* which improve convergence rate and reduce sensitivity to hyper-parameter over existing methods. We show that the algorithm is competitive against state-of-the-art first and second order methods. Our work opens up new avenues for principled algorithmic design built upon the optimal control theory.

1. Introduction

In this work, we consider the following optimal control problem (OCP) in the discrete-time setting:

$$\begin{aligned} \min_{\bar{\mathbf{u}}} J(\bar{\mathbf{u}}; \mathbf{x}_0) &:= \left[\phi(\mathbf{x}_T) + \sum_{t=0}^{T-1} \ell_t(\mathbf{x}_t, \mathbf{u}_t) \right] \text{ (OCP)} \\ \text{s.t. } \mathbf{x}_{t+1} &= f_t(\mathbf{x}_t, \mathbf{u}_t), \end{aligned}$$

where $\mathbf{x}_t \in \mathbb{R}^n$ and $\mathbf{u}_t \in \mathbb{R}^m$ represent the state and control at each time step t . $f_t(\cdot, \cdot)$, $\ell_t(\cdot, \cdot)$ and $\phi(\cdot)$ respectively denote the nonlinear dynamics, intermediate cost and terminal cost functions. OCP aims to find a control trajectory, $\bar{\mathbf{u}} \triangleq \{\mathbf{u}_t\}_{t=0}^{T-1}$, such that the accumulated cost J over the

¹Georgia Institute of Technology, Atlanta, GA 30332, USA. Correspondence to: Guan-Horng Liu <ghliu@gatech.edu>.

Preliminary work.

Table 1. Terminology Mapping

	DEEP LEARNING	OPTIMAL CONTROL
J	Total Loss	Trajectory Cost
\mathbf{x}_t	Activation Vector at Layer t	State at Time Step t
\mathbf{u}_t	Weight at Layer t	Control at Time Step t
f	Layer	Dynamical System
ϕ	End-goal Loss	Terminal Cost
l	Weight Regularization	Intermediate Cost

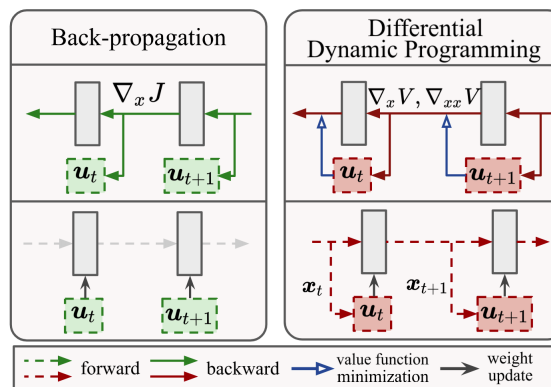


Figure 1. Computational graphs in the backward pass (upper) and weight update (lower). DDP differs from Back-propagation in that (1) the value derivatives $\nabla_x V, \nabla_{xx} V$, as opposed to the loss gradient $\nabla_x J$, are computed backward, and (2) the weight, denoted as \mathbf{u}_t , is updated using layer-wise feedback policies (shown in red as functions of state) with additional forward propagation.

finite horizon T is minimized. Problems with the form of OCP appear in multidisciplinary areas since it describes a generic multi-stage decision making problem, and have gained commensurate interest recently in deep learning.

Central to the research along this line is the interpretation of DNNs as discrete-time nonlinear dynamical systems, in which each layer is viewed as a distinct time step (Weinan, 2017). The dynamical system perspective provides mathematically-sound explanation for the success of certain DNN architectures (Lu et al., 2019). It also enables principled architecture design by bringing rich analysis from numerical differential equations (Lu et al., 2017; Long et al., 2017) and discrete mechanism (Greydanus et al., 2019; Zhong et al., 2019) when learning problems inherit

physical structures. In the continuum limit of depth, [Chen et al. \(2018\)](#) parametrized an ordinary differential equation (ODE) directly using DNNs, later with [Liu et al. \(2019\)](#) extending the framework to accept stochastic dynamics.

From the optimization viewpoint, iterative algorithms for solving OCP have been shown to admit a control interpretation ([Hu & Lessard, 2017](#)). When the network weight is recast as the control variable, OCP describes without any loss of generalization the training objective composed of layer-wise loss (e.g. weight regularization) and terminal loss (e.g. cross-entropy). This connection has been mathematically explored in many recent works ([Weinan et al., 2018](#); [Seidman et al., 2020](#); [Liu & Theodorou, 2019](#)). Despite they provide theoretical statements for convergence and generalization, the algorithmic development remains relatively limited. Specifically, previous works primarily focus on applying first-order optimality conditions, provided by the Pontryagin principle ([Boltyanskii et al., 1960](#)), to architectures restricted to residual blocks or discrete weights ([Li & Hao, 2018](#); [Li et al., 2017](#)).

In this work, we take a parallel path from the Approximate Dynamic Programming (ADP, [Bertsekas et al. \(1995\)](#)), a technique particularly designed to solve complex Markovian decision processes. For this kind of problems, ADP has been shown numerically superior to *direct* optimization such as Newton method since it takes into account the temporal structure inherit in OCP ([Liao & Shoemaker, 1992](#)). The resulting update features a locally optimal feedback policy at each stage (see Fig. 1), which is in contrast to the one derived from the Pontryagin’s principle. In the application of DNNs, we will show through experiments that the policies help improve training convergence and reduce sensitivity to hyper-parameter change.

Of our particular interest among practical ADP algorithms is the Differential Dynamic Programming (DDP, [Jacobson & Mayne \(1970\)](#)). DDP is a second order method that has been used extensively for complex trajectory optimization in robotics ([Tassa et al., 2014](#); [Posa et al., 2016](#)), and in this work we further show that existing first and second order methods for training DNNs can be derived from DDP as special cases (see Table 2). Such an intriguing connection can be beneficial to both sides. While we can leverage recent advances in efficient curvature factorization of the loss Hessian ([Martens & Grosse, 2015](#); [George et al., 2018](#)) to relieve the computational burden in DDP, on the other hand, computing feedback policies stands as an independent module; thus it can be integrated into existing first and

Notation: We will always use t as the time step of dynamics and denote a trajectory as $\bar{\mathbf{x}} \triangleq \{\mathbf{x}_t\}_{t=0}^{T-1}$. Given a function $\mathcal{F}_t : \mathbb{X} \mapsto \mathbb{U}$, we denote its Jacobian and Hessian respectively as $\nabla_{\mathbf{x}} \mathcal{F}_t \in \mathbb{R}^{\mathbb{X} \times \mathbb{U}}$ and $\nabla_{\mathbf{x}\mathbf{x}} \mathcal{F}_t \in \mathbb{R}^{\mathbb{X} \times \mathbb{X} \times \mathbb{U}}$, and sometimes abbreviate them by \mathcal{F}_x^t and \mathcal{F}_{xx}^t . Given a matrix \mathbf{A} , its element at (i, j) is denoted as $[\mathbf{A}]_{(i,j)}$, with its sub-matrix denoted as $[\mathbf{A}]_{(i,j,k:p)}$.

second order methods.

The concept of feedback mechanism has already shown up in the study of network design, where the terminology typically refers to connections between modules over training ([Chung et al., 2015](#); [Wen et al., 2018](#)) or successive prediction for vision applications ([Zamir et al., 2017](#); [Li et al., 2019](#)). Conceptually perhaps [Shama et al. \(2019\)](#); [Huh et al. \(2019\)](#) are most related to our work, where the authors proposed to reuse the discriminator from a Generative Adversarial Network as a feedback module during training or test time. We note that, however, neither the problem formulation nor the mapping space of the feedback module is the same as ours. Our feedback policy is originated from the optimal control theory in which control update needs to compensate the state disturbance throughout propagation.

The paper is organized as follows: In section 2 we go over background on optimality conditions to OCP and review the DDP algorithm. Connection between DNNs training and trajectory optimization is solidified in section 3, with a practical algorithm demonstrated in section 4. We provide empirical results and future directions in section 5 and 6.

2. Preliminaries

2.1. Optimality Conditions to OCP

Development of the optimality conditions to OCP can be dated back to 1960s, characterized by the Pontryagin’s Maximum Principle (PMP) and the Dynamic Programming (DP). We detail the two different approaches below.

Theorem 1 (Discrete-time PMP ([Todorov, 2016](#))). *Let $\bar{\mathbf{u}}^*$ be the optimal control trajectory for OCP and $\bar{\mathbf{x}}^*$ be the corresponding state trajectory. Then, there exists a co-state trajectory $\bar{\mathbf{p}}^* \triangleq \{\mathbf{p}_t^*\}_{t=1}^T$, such that*

$$\mathbf{x}_{t+1}^* = \nabla_{\mathbf{p}} H(\mathbf{x}_t^*, \mathbf{p}_{t+1}^*, \mathbf{u}_t^*), \quad \mathbf{x}_0^* = \mathbf{x}_0, \quad (1)$$

$$\mathbf{p}_t^* = \nabla_{\mathbf{x}} H(\mathbf{x}_t^*, \mathbf{p}_{t+1}^*, \mathbf{u}_t^*), \quad \mathbf{p}_T^* = \nabla_{\mathbf{x}} \phi(\mathbf{x}_T^*), \quad (2)$$

$$\mathbf{u}_t^* = \arg \min_{\mathbf{v} \in \mathbb{R}^m} H(\mathbf{x}_t^*, \mathbf{p}_{t+1}^*, \mathbf{v}). \quad (3)$$

Eq. (2) is called *adjoint equation*, and the discrete-time Hamiltonian $H : \mathbb{R}^n \times \mathbb{R}^n \times \mathbb{R}^m \mapsto \mathbb{R}$ is given by

$$H(\mathbf{x}_t, \mathbf{p}_{t+1}, \mathbf{u}_t) \triangleq \mathbf{p}_{t+1}^\top f_t(\mathbf{x}_t, \mathbf{u}_t) + \ell_t(\mathbf{x}_t, \mathbf{u}_t).$$

The discrete-time PMP theorem can be derived using KKT conditions, in which the co-state \mathbf{p}_t is equivalent to the Lagrange multiplier. As we will see in section 3.1, the adjoint dynamics Eq. (2) has a direct link to the Back-propagation. Note that the solution to Eq. (3) admits an open-loop process in the sense that it does not depend on state variables. This is in contrast to the Dynamic Programming (DP) principle, in which a feedback policy is considered.

Theorem 2 (DP (Bellman, 1954)). Define a value function $V_t : \mathbb{R}^n \mapsto \mathbb{R}$ at each time step, computed backward in time using the Bellman equation

$$V_t(\mathbf{x}_t) = \min_{\mathbf{u}_t \in \Gamma} \{ \ell_t(\mathbf{x}_t, \mathbf{u}_t) + V_{t+1}(f_t(\mathbf{x}_t, \mathbf{u}_t)) \}, \quad (4)$$

with $V_T(\mathbf{x}_T) = \phi(\mathbf{x}_T)$. $\Gamma : \mathbb{R}^n \mapsto \mathbb{R}^m$ denotes a set of mapping from state to control space. Then, we have $V_0(\mathbf{x}_0) = J^*(\mathbf{x}_0)$ be the optimal objective value to OCP. Furthermore, if $\mathbf{u}_t^* = \mu_t^*(\mathbf{x}_t)$ minimizes the RHS of Eq. (4), then the policy $\pi^* = \{\mu_0^*, \dots, \mu_{T-1}^*\}$ is optimal.

Hereafter we denote the objective involved at each decision stage in Eq. (4) as the *Bellman objective* $Q_t(\mathbf{x}_t, \mathbf{u}_t)$:

$$Q_t(\mathbf{x}_t, \mathbf{u}_t) \triangleq \ell_t(\mathbf{x}_t, \mathbf{u}_t) + V_{t+1}(f_t(\mathbf{x}_t, \mathbf{u}_t)). \quad (5)$$

The principle of DP recasts the problem of minimizing over a control sequence to a sequence of minimization over each control. The value function V_t summarizes the optimal cost-to-go at each stage, provided the following control subsequence also being optimal. $\bar{\mathbf{u}}^*(\bar{\mathbf{x}})$ is an optimal feedback law in a globally convergent closed loop system.

2.2. Differential Dynamic Programming

Trajectory optimization algorithms typically rely on solving the optimality equations from PMP or DP. Unfortunately, solving the Bellman equation in high-dimensional problems is infeasible without any approximation, well-known as the Bellman curse of dimensionality. To mitigate the computational burden from the minimization involved at each stage, one can replace the Bellman objective in Eq. (4) with its second order approximation. Such an approximation is central to the Differential Dynamic Programming (DDP), a second-order method that inherits a similar Bellman optimality structure while being computationally efficient.

Given a nominal trajectory $(\bar{\mathbf{x}}, \bar{\mathbf{u}})$, DDP iteratively optimizes its accumulated cost, where each iteration consists a backward and forward pass, detailed below.

Backward pass: At each time step, DDP expands Q_t at $(\mathbf{x}_t, \mathbf{u}_t)$ up to second-order, i.e. $Q_t(\mathbf{x}_t + \delta\mathbf{x}_t, \mathbf{u}_t + \delta\mathbf{u}_t) \approx Q_t(\mathbf{x}_t, \mathbf{u}_t) + \delta Q_t(\delta\mathbf{x}_t, \delta\mathbf{u}_t)$, where δQ_t is expanded as¹

$$\delta Q_t = \frac{1}{2} \begin{bmatrix} 1 \\ \delta\mathbf{x}_t \\ \delta\mathbf{u}_t \end{bmatrix}^\top \begin{bmatrix} 0 & Q_x^\top & Q_u^\top \\ Q_x & Q_{xx} & Q_{xu} \\ Q_u & Q_{ux} & Q_{uu} \end{bmatrix} \begin{bmatrix} 1 \\ \delta\mathbf{x}_t \\ \delta\mathbf{u}_t \end{bmatrix}$$

with each term given by

$$Q_x = \ell_x + f_x^\top V_{x'}' \quad (6a)$$

$$Q_u = \ell_u + f_u^\top V_{x'}' \quad (6b)$$

$$Q_{xx} = \ell_{xx} + f_x^\top V_{x'x'}' f_x + V_{x'}' \cdot f_{xx} \quad (6c)$$

¹ We drop the time step t in all derivatives of Q for simplicity.

$$Q_{uu} = \ell_{uu} + f_u^\top V_{x'x'}' f_u + V_{x'}' \cdot f_{uu} \quad (6d)$$

$$Q_{ux} = \ell_{ux} + f_u^\top V_{x'x'}' f_x + V_{x'}' \cdot f_{ux} \quad (6e)$$

$V_{x'}' \triangleq \nabla_x V_{t+1}(\mathbf{x}_{t+1})$ denotes the derivative of the value function at the next state. The dot notation in Eq. (6c) - (6e) represents the product of a vector with a 3D tensor. The optimal perturbation to this approximate Bellman objective admits an analytic form given by

$$\delta\mathbf{u}_t^*(\delta\mathbf{x}_t) = \mathbf{k}_t + \mathbf{K}_t \delta\mathbf{x}_t, \quad (7)$$

where $\delta\mathbf{x}_t = \mathbf{x}_t^* - \mathbf{x}_t$. $\mathbf{k}_t \triangleq -Q_{uu}^{-1} Q_{ux}$ and $\mathbf{K}_t \triangleq -Q_{uu}^{-1} Q_{ux}$ respectively denote the open and feedback gains. Note that this policy is only optimal locally around the nominal trajectory where the second order approximation remains valid. The backward pass repeats the computation Eq. (6) - (7) backward in time, with the first and second derivative of value function computed also recursively by

$$\begin{aligned} V_x^t &= Q_x - Q_{ux}^\top Q_{uu}^{-1} Q_u \\ V_{xx}^t &= Q_{xx} - Q_{ux}^\top Q_{uu}^{-1} Q_{ux} \end{aligned} \quad (8)$$

Forward pass: In the forward pass, we simply simulate a trajectory by applying the feedback policy computed at each stage. Then, a new Bellman objective Q is expanded along the updated trajectory, and the whole procedure repeats until the termination condition is met. Under mild assumptions, DDP admits quadratic convergence for systems with smooth dynamics (Mayne, 1973) and is numerically superior to Newton's method (Liao & Shoemaker, 1992). We summarize the DDP algorithm in Alg. 1.

3. Training DNNs as Trajectory Optimization

3.1. Optimal Control Formulation

Recall that DNNs can be interpreted as dynamical systems in which each layer is viewed as a distinct time step. Consider for instance the mapping in feedforward networks,

$$\mathbf{x}_{t+1} = \sigma_t(\mathbf{h}_t) \quad \mathbf{h}_t = g_t(\mathbf{x}_t, \mathbf{u}_t) \equiv \mathbf{W}_t \mathbf{x}_t + \mathbf{b}_t. \quad (9)$$

$\mathbf{x}_t \in \mathbb{R}^{n_t}$ and $\mathbf{x}_{t+1} \in \mathbb{R}^{n_{t+1}}$ represent the activation at layer t and $t+1$, with $\mathbf{h}_t \in \mathbb{R}^{n_{t+1}}$ being the pre-activation. σ_t and g_t respectively denote the nonlinear activation function and the affine transform parametrized by the weight $\mathbf{u}_t \triangleq [\text{vec}(\mathbf{W}_t), \mathbf{b}_t]^\top$. Eq. (9) can be seen as a dynamical system propagating the activation vector \mathbf{x}_t using \mathbf{u}_t .

It is natural to ask whether the necessary condition in the PMP theorem relates to first-order optimization methods in DNN training. This is indeed the case as pointed out in Li et al. (2017) and Liu & Theodorou (2019).

Lemma 3 (Li et al., 2017)). *Back-propagation with gradient descent satisfies Eq. (2) and iteratively solves the minimization described by Eq. (3).*

Algorithm 1 Differential Dynamic Programming

Input: nominal trajectory $\{\bar{\mathbf{x}}_{\text{nom}}, \bar{\mathbf{u}}_{\text{nom}}\}$
repeat
 Set $V_x^T = \nabla_x \phi$ and $V_{xx}^T = \nabla_{xx} \phi$
for $t = T - 1$ **to** 0 **do**
 Compute $Q_x^t, Q_u^t, Q_{xx}^t, Q_{ux}^t, Q_{uu}^t$ with Eq. (6)
 Compute feedback policy $\delta \mathbf{u}_t^*(\delta \mathbf{x}_t)$ with Eq. (7)
 Compute V_x^t, V_{xx}^t with Eq. (8)
end for
 Set $\mathbf{x}_0^* = \mathbf{x}_0$
for $t = 0$ **to** $T - 1$ **do**
 $\mathbf{u}_t^* = \mathbf{u}_t + \mathbf{k}_t + \mathbf{K}_t(\delta \mathbf{x}_t)$, where $\delta \mathbf{x}_t = \mathbf{x}_t^* - \mathbf{x}_t$
 $\mathbf{x}_{t+1}^* = f_t(\mathbf{x}_t^*, \mathbf{u}_t^*)$
end for
 $\{\bar{\mathbf{x}}_{\text{nom}}, \bar{\mathbf{u}}_{\text{nom}}\} \leftarrow \{\bar{\mathbf{x}}^*, \bar{\mathbf{u}}^*\}$
until terminate condition is met

Lemma 3 follows by expanding the RHS of Eq. (1) and (2):

$$\begin{aligned} \nabla_{\mathbf{p}_{t+1}} H(\mathbf{x}_t, \mathbf{p}_{t+1}, \mathbf{u}_t) &= f_t(\mathbf{x}_t, \mathbf{u}_t), \\ \nabla_{\mathbf{x}_t} H(\mathbf{x}_t, \mathbf{p}_{t+1}, \mathbf{u}_t) &= \nabla_{\mathbf{x}_t} f_t(\mathbf{x}_t, \mathbf{u}_t)^\top \mathbf{p}_{t+1} \\ &\quad + \nabla_{\mathbf{x}_t} \ell_t(\mathbf{x}_t, \mathbf{u}_t) = \nabla_{\mathbf{x}_t} J(\bar{\mathbf{u}}; \mathbf{x}_0). \end{aligned}$$

Thus, the first two equations in PMP correspond to the forward propagation and the chain rule used for Back-propagation. Notice that we now have the subscript t in the gradient since the dimension of \mathbf{x}_t and \mathbf{p}_t may change with time. When the Hamiltonian is differentiable wrt \mathbf{u}_t , one can attempt to solve Eq. (3) by iteratively taking the gradient descent. This will lead to the familiar update:

$$\begin{aligned} \mathbf{u}_t^{(k+1)} &= \mathbf{u}_t^{(k)} - \eta \nabla_{\mathbf{u}_t} H(\mathbf{x}_t, \mathbf{p}_{t+1}, \mathbf{u}_t) \\ &= \mathbf{u}_t^{(k)} - \eta (\nabla_{\mathbf{u}_t} f_t(\mathbf{x}_t, \mathbf{u}_t)^\top \mathbf{p}_{t+1} + \nabla_{\mathbf{u}_t} \ell_t(\mathbf{x}_t, \mathbf{u}_t)) \\ &= \mathbf{u}_t^{(k)} - \eta \nabla_{\mathbf{u}_t} J(\bar{\mathbf{u}}; \mathbf{x}_0), \end{aligned} \quad (10)$$

where k and η denote the update iteration and step size.

We now extend Lemma 3 to accept the batch setting. The following proposition will become useful as we proceed to the algorithm design in the next section.

Proposition 4. (Informal; see Appendix A for full version) Let $\mathbf{X}_t \triangleq \{\mathbf{x}_t^{(i)}\}_{i=1}^B \in \mathbb{R}^{Bn_t}$ denote the augmented state with the batch size B . Consider the new objective $\mathbf{J}(\bar{\mathbf{u}}; \mathbf{X}_0) \triangleq \frac{1}{B} \sum_B J(\bar{\mathbf{u}}; \mathbf{x}_0^{(i)})$. Then, iteratively solving the ‘‘augmented’’ PMP equations is equivalent to applying mini-batch gradient descent with Back-propagation. Specifically, the derivative of the augmented Hamiltonian \mathbf{H} takes the exact form with the mini-batch gradient update:

$$\nabla_{\mathbf{u}_t} \mathbf{H}(\mathbf{X}_t, \mathbf{P}_{t+1}, \mathbf{u}_t) = \frac{1}{B} \sum_B \nabla_{\mathbf{u}_t} J(\bar{\mathbf{u}}; \mathbf{x}_0^{(i)}), \quad (11)$$

where $\mathbf{P}_{t+1} = \frac{1}{B} [\mathbf{p}_{t+1}^{(1)}, \dots, \mathbf{p}_{t+1}^{(B)}]^\top$.

Algorithm 2 Back-propagation with Gradient Descent

Input: nominal trajectory $\{\bar{\mathbf{x}}_{\text{nom}}, \bar{\mathbf{u}}_{\text{nom}}\}$, learning rate η
 Set $\mathbf{p}_T = \nabla_x \phi$
for $t = T - 1$ **to** 0 **do**
 $\delta \mathbf{u}_t = \nabla_{\mathbf{u}_t} H = \nabla_{\mathbf{u}_t} \{\sigma_t(g_t(\mathbf{x}_t, \mathbf{u}_t))\}^\top \mathbf{p}_{t+1} + \nabla_{\mathbf{u}_t} \ell_t$
 $\mathbf{p}_t = \nabla_{\mathbf{x}_t} H = \nabla_{\mathbf{x}_t} \{\sigma_t(g_t(\mathbf{x}_t, \mathbf{u}_t))\}^\top \mathbf{p}_{t+1} + \nabla_{\mathbf{x}_t} \ell_t$
end for
 $\mathbf{u}_t \leftarrow \mathbf{u}_t - \eta \delta \mathbf{u}_t, \quad \forall t \in \{0, 1, \dots, T - 1\}$

Proposition 4 suggests that in the batch setting, we aim to find an ultimate open-loop control that can drive every initial state among the batch data to its designed target. Despite seemingly trivial, this is a distinct formulation to OCP since the optimal policy typically varies at different initial state.

It should be stressed that despite the appealing connection between the optimal control and DNN training, the two methodologies are not completely interchangeable. We note that the dimension of the activation typically changes throughout layers to extract effective latent representation. This unique property poses difficulties when one wish to adopt analysis from the continuous-time framework. Despite the recent attention on treating networks as an discretization of ODE (Lu et al., 2017; Weinan et al., 2018), we note that this formulation restricts the applicability of the optimal control theory to networks with residual architectures, as opposed to the generic dynamics discussed here.

3.2. Trajectory Optimization Perspective

In this part we draw a new connection between the training procedure of DNNs and trajectory optimization. Let us first revisit the Back-propagation with gradient descent from Alg. 2. During the forward propagation, we treat the weight as the *nominal control* $\bar{\mathbf{u}}$ that simulates the state trajectory $\bar{\mathbf{x}}$. Then, the loss gradient is propagated backward, implicitly moving in the direction suggested by the Hamiltonian. The control update, in this case the first-order derivative, is computed simultaneously and later applied to the system.

It should be clear at this point that Alg. 2 resembles DDP in several ways. Starting from the nominal trajectory, both procedures carry certain information wrt the objective, either \mathbf{p}_t or $\{V_x^t, V_{xx}^t\}$, backward in time in order to compute the control update. Since DDP computes the feedback policy at each time step, additional forward simulation is required in order to apply the update. The computation graph for the two processes is summarized in Fig. 1. In the following proposition we make this connection formally and provide conditions when the two algorithms become equivalent.

Proposition 5. Assume $Q_{\mathbf{u}\mathbf{x}}^t = \mathbf{0}$ at all stages, then the dynamics of the value derivative can be described by the adjoint dynamics, i.e. $V_x^t = \mathbf{p}_t, \forall t$. In this case, DDP is

Table 2. Connection between existing algorithms and DDP

	1ST-ORDER	ADAPTIVE 1ST-ORDER	STAGE-WISE NEWTON
Q_{uu}^{-1}	$\eta \mathbf{I}$	$\eta \text{diag}(g)$	J_{uu}^{-1}
Q_{ux}	$\mathbf{0}$	$\mathbf{0}$	$\mathbf{0}$

equivalent to the stage-wise Newton by having

$$Q_u^t = H_u^t = \nabla_{u_t} J, \quad Q_{uu}^t = \nabla_{u_t u_t} J, \quad \forall t. \quad (12)$$

If furthermore we have $(Q_{uu}^t)^{-1} = \eta \mathbf{I}_{m_t}$, then DDP degenerates to the Back-propagation with gradient descent.

We leave the full proof in Appendix C and provide some intuitions for the connection between first-order derivatives. First, notice that we always have $p_T = V_x^T = \nabla_x \phi$ at the horizon T without any assumption. It can be shown by induction that when $Q_{ux}^t = \mathbf{0}$ for all the remaining stages, p_t will take the same update equation with V_x^t ,

$$\begin{aligned} p_t &= H_x^t = \ell_x^t + f_x^{t\top} p_{t+1} \\ V_x^t &= Q_x^t - Q_{ux}^{t\top} (Q_{uu}^t)^{-1} Q_u^t = \ell_x^t + f_x^{t\top} V_{x'}^t, \end{aligned}$$

and Eq. (12) follows immediately by

$$Q_u^t = \ell_u^t + f_u^{t\top} V_{x'}^t = \ell_u^t + f_u^{t\top} p_{t+1} = H_u^t = \nabla_{u_t} J.$$

The feedback policy under this assumption degenerates to

$$\begin{aligned} \delta u_t^*(\delta x_t) &= -(Q_{uu}^t)^{-1} (Q_u^t + Q_{ux}^t \delta x_t) \\ &= -\nabla_{u_t u_t} J^{-1} \nabla_{u_t} J, \end{aligned}$$

which is equivalent to the stage-wise Newton method (DE O. PANTOJA, 1988). It can be readily seen that we will recover the gradient descent update by having an isotropic inverse covariance, $(Q_{uu}^t)^{-1} = \eta \mathbf{I}_{m_t}$.

Proposition 5 states that the backward pass in DDP collapses to the Back-propagation when Q_{ux} vanishes. To better explain the role of Q_{ux} during optimization, consider an illustrated 2D example in Fig. 2. Given an arbitrary objective L expanded at (x, u) , standard second-order methods compute the Hessian wrt u and apply the update $-L_{uu}^{-1} L_u$. DDP differs from them in that it also computes the *mixed* partial derivatives, i.e. L_{ux} . The resulting update law has the same update but with an additional term linear in state. This feedback term, shown in the red arrow, compensates when the state moves apart from x during update. In Sec. 5.2, we will conduct ablation study and discuss the effect of this deviation δx on DNNs training. Connection between DDP and existing methods is summarized in Table 2.

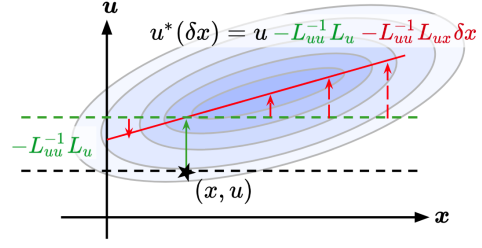


Figure 2. A toy illustration on the difference between the open loop and closed loop policy, denoted with green and red. The contour represents the objective L expanded at (x, u) . The feedback policy in this case is a line lying at the valley of the objective.

4. DDP Optimizer for Feedforward Networks

In this section we discuss a practical implementation of DDP on training feedforward networks. Due to space constraint, we leave the complete derivation in the Appendix B.

4.1. Batch DDP Formulation

We first derive the differential Bellman objective δQ when feedforward networks are used as the dynamics. Recall the propagation formula in Eq. (9) and substitute this new dynamics to the OCP by setting $f_t \equiv \sigma_t \circ g_t$. After some algebra, we can show that²

$$\begin{aligned} Q_x &= \ell_x + g_x^T V_h, \quad Q_u = \ell_u + g_u^T V_h \\ Q_{xx} &= \ell_{xx} + g_x^T (V_{hh} + V_{x'}^T \cdot \sigma_{hh}) g_x + V_h \cdot g_{xx} \\ Q_{uu} &= \ell_{uu} + g_u^T (V_{hh} + V_{x'}^T \cdot \sigma_{hh}) g_u + V_h \cdot g_{uu} \\ Q_{ux} &= \ell_{ux} + g_u^T (V_{hh} + V_{x'}^T \cdot \sigma_{hh}) g_x + V_h \cdot g_{ux} \end{aligned} \quad (13)$$

where $V_h \triangleq \sigma_h^T V_{x'}$ and $V_{hh} \triangleq \sigma_h^T V_{x' x'} \sigma_h$ denote the derivatives of the value function at pre-activation. Computing the layer-wise feedback policy and the value function remain the same as in Eq. (7) and (8).

The computational overhead in Eq. (13) can be mitigated by leveraging the structure of feedforward networks. Since the affine transform is bilinear in x and u , the terms g_{xx} and g_{uu} vanish. The tensor g_{ux} admits a sparse structure. For fully-connected layers, computation can be simplified to

$$\begin{aligned} [g_{ux}]_{(i,j,k)} &= 1 \quad \text{iff} \quad j = (k-1)n_{t+1} + i, \\ [V_h \cdot g_{ux}]_{((k-1)n_{t+1}:kn_{t+1},k)} &= V_h. \end{aligned} \quad (14)$$

For the coordinate-wise nonlinear transform, σ_h and σ_{hh} are diagonal matrix and tensor. In most learning instances, stage-wise losses typically involved with weight decay alone; thus the terms $\ell_x, \ell_{xx}, \ell_{ux}$ also vanish.

Note that Eq. (13) describes the δQ expansion along a *single* trajectory with the dynamics given by the feedforward

² We omit the subscript t again for simplicity.

networks. To modify it in the setting of batch trajectories optimization, we augment the activation space to $\mathbf{X}_t \in \mathbb{R}^{Bn_t}$ (recall B is the batch size), in the spirit of Proposition 4. It should be stressed, however, that despite drawing inspiration from the augmented Hamiltonian framework, the resulting representation does not admit a clean form such as averaging over individual updates in Eq. (11). To see why this is the case, observe that at the horizon T , the derivative of the augmented value function can indeed be expressed by the individual ones by $\mathbf{V}_X^T = \frac{1}{B} [\dots V_{x^{(i)}}^T \dots]^T$. Such an independent structure does not preserve through the backward pass since at $t = T - 1$, \mathbf{V}_X^{T-1} instead takes the form

$$\mathbf{V}_X^{T-1} = \frac{1}{B} \begin{bmatrix} \vdots \\ Q_{x^{(i)}}^{T-1} \\ \vdots \end{bmatrix} - \frac{1}{B} \begin{bmatrix} \vdots \\ Q_{ux^{(i)}}^{T-1} \\ \vdots \end{bmatrix}^T (\mathbf{Q}_{uu}^{T-1})^{-1} \mathbf{Q}_u^{T-1},$$

where \mathbf{Q}_{uu}^{T-1} and \mathbf{Q}_u^{T-1} are the averaging over $Q_{uu}^t | x_t^{(i)}$ and $Q_u^t | x_t^{(i)}$. The intuition is that when optimizing batch trajectories with the *same* control law, the Bellman objective of each sample couples with others through the second order expansion of the augmented \mathbf{Q} . Consequently, the value function will no longer be independent soon after leaving the terminal horizon. We highlight this trait which distinguishes batch DDP from its original representation.

4.2. Practical Implementation

Directly applying the batch DDP to optimize DNNs can be impractical. For one, training inherits stochasticity due to mini-batch sampling. This differs from standard trajectory optimization where the initial state remains unaltered throughout optimization. Secondly, the control dimension is typically order of magnitude higher than the one for state; thus inverting the Hessian Q_{uu} soon becomes computationally infeasible. In this part we discuss several practical implementation adopted from both literature that stabilizes the optimization process and enables real-time training.

First, we apply Tikhonov regularization on Q_{uu} and line search since both play key roles in the convergence of DDP (Liao & Shoemaker, 1991). We note that these regularization have shown up already in robustifying DNNs training, with the form of l_2 -norm and in Vaswani et al. (2019). From the perspective of trajectory optimization, we should emphasize that without regularization, Q_{uu} will lose its positive definiteness whenever $f_u^T V_{x'x'}^T f_u$ has a low rank. This is indeed the case in feedforward networks. The observation on low-rank matrices also applies to $f_x^T V_{x'x'}^T f_x$ when the dimension of the activation reduces during forward propagation. Thus we also apply Tikhonov regularization to V_{xx} . This can be seen as placing a quadratic state-cost and has been shown to improve robustness on optimizing complex humanoid (Tassa et al., 2012). Next, when using DDP for

trajectory optimization, one typically has the option of expanding the dynamics up to first or second order. Note that both are still considered second-order methods and generate layer-wise feedback policies, except the former simplifies the problem similar to Gauss-Newton. The computational benefit and stability obtained by keeping only the linearized dynamics have been discussed thoroughly in robotics literature (Todorov & Li, 2005; Tassa et al., 2012). Thus, hereafter we will refer the DDP optimizer to this version.

Tremendous efforts have been spent recently on efficient curvature estimation of the loss landscape during training. This is particularly crucial in enabling the applicability of the second-order methods, since inverting the full Hessian $J_{\bar{u}\bar{u}}$, even in a layer-wise fashion, can be computationally intractable, and DDP has no exception. Fortunately, DDP can be integrated with these advances. We first notice that many popular curvature factorization methods contain modules that collect certain statistics during training to compute the preconditioned update. Take EKFac (George et al., 2018) for instance, the update for each layer is approximated by $J_{u_t u_t}^{-1} J_{u_t} \approx \text{CurvApprox}(J_{u_t}; \{x_t, J_{h_t}\}_{k=0}^K)$, where $\{\cdot\}_{k=0}^K$ denotes the history until the most recent iteration K . The module bypasses the computation of Hessian and its inverse by directly estimating the matrix-vector product. We can integrate CurvApprox with DDP by

$$(Q_{uu}^t)^{-1} Q_u^t \approx \text{CurvApprox}(Q_u^t; \{x_t, V_{h_t}^t\}_{k=0}^K), \quad (15)$$

and compute $Q_{uu}^{-1} Q_{ux}$ by applying Eq. (15) column-wise. Notice that we replace J_{h_t} with V_{h_t} since here we aim to approximate the landscape of the value function. Hereafter we name this approximation by *DDP-EKFac*.

Integrating DDP with existing optimizers is not restricted to second-order methods. Recall the connection we made in Proposition 5. When Q_{uu}^{-1} is isotropic, DDP inherits the same structure as gradient descent. In a similar vein, adaptive first order methods, such as RMSprop (Hinton et al., 2012), approximate Q_{uu}^{-1} by $\text{diag}(g)$, where g adapting to the diagonal of the inverse covariance. We will refer these two variants to *DDP-SGD* and *DDP-RMSprop*.

5. Experiments

5.1. Batch Trajectory Optimization on Synthetic Data

We first demonstrate the effectiveness of our DDP optimizer in batch trajectories optimization. Recall from the derivation in Sec. 2.2 that the feedback policy is optimal locally around the region where Q is expanded; thus only samples traveling through this region benefits. Since conceptually a DNN classifier can be thought of as a dynamical system guiding each group of trajectories toward the region belong to their classes, we hypothesize that for the DDP optimizer to show its effectiveness on batch training, the feedback policy must

Table 3. Performance Comparison on Train Loss and Test Accuracy (%).

DATA SET	SGD	RMSPROP	KFAC	EKFAC	KWNG	DDP SGD	DDP RMSPROP	DDP EKFAC	DDP
WINE	0.5654 (94.35)	0.5515 (98.10)	0.5601 (97.78)	0.5610 (94.60)	0.5565 (98.67)	0.5657 (94.29)	0.5515 (98.10)	0.5610 (94.60)	0.5649 (98.00)
IRIS	0.0514 (93.00)	0.0942 (91.48)	0.0588 (94.28)	0.0514 (94.86)	0.0673 (94.07)	0.0505 (93.79)	0.0515 (94.81)	0.0567 (92.72)	0.0552 (94.44)
DIGITS	0.0400 (95.28)	0.0562 (94.52)	0.4474 (84.61)	0.0864 (94.53)	0.1321 (93.83)	0.0364 (95.43)	0.0450 (94.71)	0.0666 (95.36)	0.2197 (91.94)
MNIST	0.2321 (92.60)	0.2742 (91.30)	0.2964 (92.02)	0.2392 (92.79)	0.3689 (88.92)	0.2242 (92.84)	0.2291 (92.42)	0.2365 (92.67)	N/A
FASHION MNIST	0.4695 (82.48)	0.4202 (84.24)	0.4572 (84.27)	0.4257 (84.14)	0.4518 (84.02)	0.4717 (82.46)	0.4191 (84.2)	0.4204 (84.39)	N/A

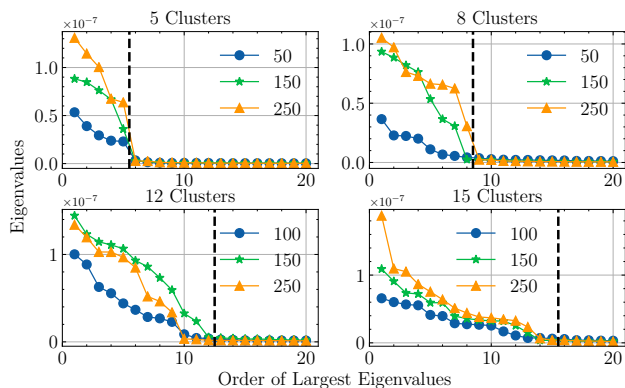


Figure 3. Spectrum distribution of the last-layer feedback policy on synthetic data, with the legend denoted each training snapshot. The vertical dashed line represents our predicted cutoff number when the policy degenerates.

act as an ensemble to capture the feedback behavior for each class. To this end, we randomly generate synthetic data points from $k \in \{5, 8, 12, 15\}$ Gaussian clusters in the input space \mathbb{R}^{30} and train a 3-layers feedforward networks (30-20-20- k) from scratch using DDP optimizer. For all settings, training error drops to nearly zero. The spectrum distribution, sorted in a descending order, of the feedback policy in the prediction layer is shown in Fig. 3. The result shows that the number of nontrivial eigenvalues in $\mathbf{Q}_{uu}^{-1} \mathbf{Q}_{uX}$ matches exactly the number of classes in each problem (indicated by the vertical dashed line). As the state distribution concentrates to k bulks through training, the eigenvalues also increase, providing stronger feedback direction to the weight update. Thus, we consolidate our batch DDP formulation in Sec. 4.1.

5.2. Performance on Classification Data Set

Next, we validate the performance of the DDP optimizer, along with several variants proposed in the previous section, on classification tasks. In addition to the baselines such as SGD and RMSprop (Hinton et al., 2012), we com-

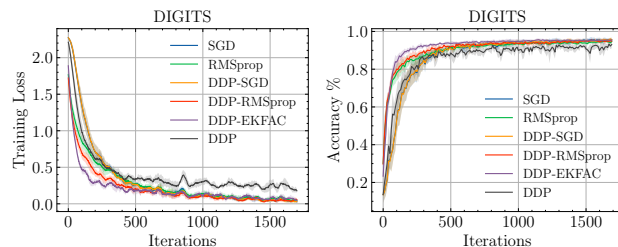


Figure 4. Performance on DIGIS. We report DDP-integrated optimizers and the other top two methods.

pare with state-of-the-art second order optimizers, including KFAC (Martens & Grosse, 2015), EKFAC (George et al., 2018), and KWNG (Arbel & Montufar, 2020). We use (fully-connected) feedforward networks for all experiments. The complete experiment setup and additional results (e.g. accuracy curve) are provided in the Appendix D. Table 3 summarizes the performance with the top two results highlighted. Without any factorization, we are not able to obtain result for DDP on (Fashion)-MNIST due to the exploding computation when inverting \mathbf{Q}_{uu} .

On all data set, DDP achieves better or comparable results against existing methods. Notably, when comparing the vanilla DDP with its approximate variants (see Fig. 4), the latter typically admit smaller variance and sometimes converge to better local minima. The instability in the former can be caused by the overestimation of the value Hessian when using only mini-batch data, which is mitigated by the amortized method used in EKFAC, or diagonal approximation in first-order methods. This shed light on the benefit gained by bridging two seemingly disconnected methodologies.

5.3. Effect of Feedback Policies

Sensitivity to Hyper-parameter: For optimizers that are compatible with DDP, we observe minor improvements over the final training loss. To better understand the effect of the feedback mechanism, we conduct ablation analysis and com-

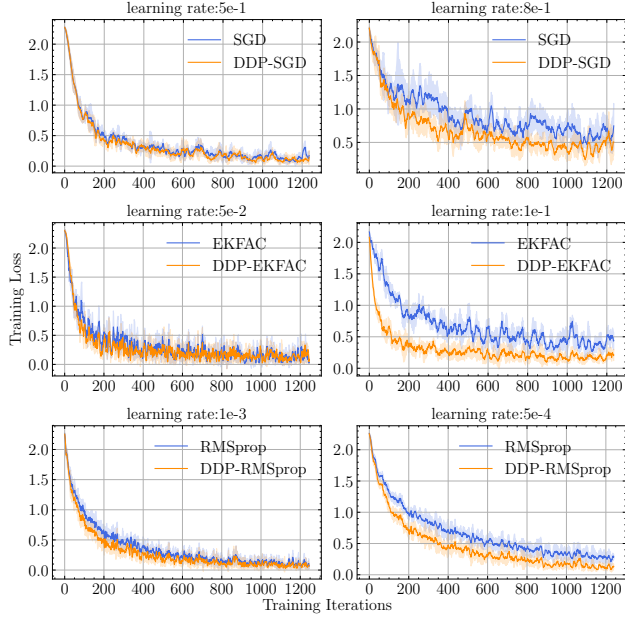


Figure 5. Ablation study on existing optimizers and their DDP versions over different learning rate. The feedback mechanism helps stabilize the training when the learning rate is perturbed from the best tuned value (shown in the left column).

pare their training performance among different learning rate setup, while keeping all the other hyper-parameters the same. The result on DIGITS is shown in Fig. 5, where the left and right columns correspond to the best-tuned and perturbed learning rate. While all optimizers are able to converge to low training error when best-tuned, the ones integrated with DDP tend to stabilize the training when the learning rate changes by some fraction; sometimes they also achieve lower training error in the end. The performance improvement induced by the feedback policy typically becomes obvious when the learning rate increases.

Variance Reduction and Faster Convergence: Table 4 shows the variance differences in training loss and test accuracy after the optimizers are integrated with DDP feedback modules. Specifically, we report the value $(\text{Var}_{\text{DDP-Alg}} - \text{Var}_{\text{Alg}}) / \text{Var}_{\text{Alg}}$, with Alg being optimizers compatible with DDP, including SGD, RMSprop, and EKFAC. We keep all hyper-parameters the same for each experiment so that the performance difference only comes from the existence of feedback policies. As shown in Table 4, for most cases having additional updates from DDP stabilizes the training dynamics by reducing its variance, and similar reduction can be observed in the variance of testing accuracy over optimization, sometimes by a large margin. Empirically, we find that such a stabilization may also lead to faster convergence. In Fig. 7, we report the training dynamics of the top three experiment instances in Table 4 that have large variance reduction when using DDP. In all cases, the optimization

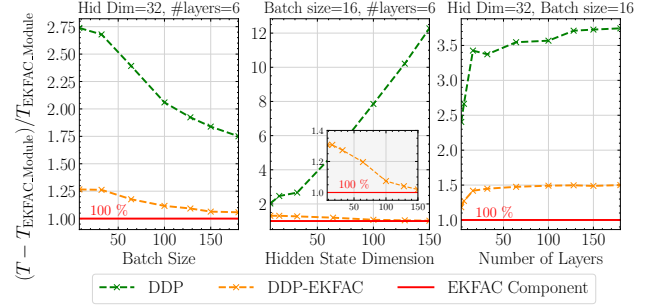


Figure 6. Overhead in the DDP backward pass compared with the computation spent on EKFAC curvature approximation (red line). We leave out the DDP curve in the middle inner plot to better visualize the overhead in DDP-EKFAC wrt hidden dimension.

paths also admit faster convergence.

To give an explanation from the trajectory optimization viewpoint, recall that DDP computes layer-wise policies with each composed of two terms. The open-loop control is state-independent and, in this setup, equivalent to the original update computed by each optimizer. The feedback term is linear in $\delta \mathbf{x}_t$, which can be expressed by $\delta \mathbf{x}_t = \tilde{f}_{0:t}(\mathbf{x}_0, \mathbf{u}_{0:t}^{(k+1)}) - \tilde{f}_{0:t}(\mathbf{x}_0, \mathbf{u}_{0:t}^{(k)})$, where we abuse the notation and denote $\tilde{f}_{0:t}$ as the compositional dynamics propagating \mathbf{x}_0 with $\mathbf{u}_{0:t} \triangleq \{\mathbf{u}_i\}_{i=0}^t$. In other words, $\delta \mathbf{x}_t$ captures the state differential when new control is applied until layer t , and we should expect it to increase when a further step size, thus a larger difference between controls, is taken at each layer. This implies the control update in the later layer may not be optimal (at least from the trajectory optimization viewpoint) since the gradient is evaluated at \mathbf{x}_t instead of $\mathbf{x}_t^* \triangleq \mathbf{x}_t + \delta \mathbf{x}_t$. The difference between $\nabla_{\mathbf{u}_t} J(\mathbf{x}_t, \mathbf{u}_t)$ and $\nabla_{\mathbf{u}_t} J(\mathbf{x}_t^*, \mathbf{u}_t)$ cannot be neglected especially during early training when the objective landscape contains nontrivial curvature everywhere (Alain et al., 2019). The feedback direction is designed to mitigate this gap. In fact we can show that $\mathbf{K}_t \delta \mathbf{x}_t$ approximately solves

$$\arg \min_{\Gamma(\delta \mathbf{x}_t)} \|\nabla_{\mathbf{u}_t} J(\mathbf{x}_t^*, \mathbf{u}_t + \delta \mathbf{u}_t) - \nabla_{\mathbf{u}_t} J(\mathbf{x}_t, \mathbf{u}_t)\|, \quad (16)$$

with the derivation provided in the Appendix C. Thus, by having this additional term throughout updates, we stabilize the training dynamics by traveling through the landscape cautiously without going off the cliff.

5.4. Remarks on Computation Overhead

Lastly, Fig. 6 summarizes the computational overhead during DDP backward pass on DIGITS. Specifically, we compare the wall-clock processing time of DDP-EKFAC and DDP to the computation spent on the curvature approximate module in the DDP-EKFAC optimizer. The value thus sug-

Table 4. Variance differences on training loss (test accuracy) after optimizers are integrated with DDP. Negative value indicates a reduction of variance over optimization and vice versa.

DATA SET	SGD vs DDP-SGD	RMSPROP vs DDP-RMSPROP	EKFAC vs DDP-EKFAC
WINE	-1.312% (-0.732%)	9.263% (-1.813%)	0.179% (0.177%)
IRIS	-2.474% (-4.021%)	1.038% (-1.854%)	-4.601% (-0.713%)
DIGITS	-1.514% (-6.743%)	-3.165% (-6.468%)	-9.020% (-39.971%)
MNIST	0.331% (-5.263%)	-1.352% (-32.503%)	-0.216% (6.344%)
FMNIST	-1.324% (-4.767%)	3.464% (20.254%)	-2.327% (4.443%)

gests the additional overhead required for EKFAC to adopt the DDP framework, which includes second-order expansion on the value function, computing layer-wise feedback policies, etc. While the vanilla batch DDP scales poorly with the dimension of the hidden state under the current batch formulation, the overhead in DDP-EKFAC increases only by a *constant* (from 1.1 to 1.6) wrt different architecture setup, such as batch size, hidden dimension, and network depth. We stress that our current implementation is not fully optimized, so there is still room for further acceleration.

6. Conclusion

In this work, we introduce Differential Dynamic Programming Neural Optimizer (DDP), a new class of algorithms arising from bridging DNNs training to the optimal control theory and trajectory optimization. This new perspective suggests existing methods stand as special cases of DDP and can be extended to adapt the framework painlessly. The resulting optimizer features layer-wise feedback policies which help reduce sensitivity to hyper-parameter and sometimes improve convergence. We wish this work provides new algorithmic insight and bridges communities from both deep learning and optimal control. There are numerous future directions left for explored. For one, deriving update laws for other architectures (e.g. convolution and batch-norm) and applying factorization to other gigantic matrices are essential to the applicability of DDP optimizer.

References

- Alain, G., Roux, N. L., and Manzagol, P.-A. Negative eigenvalues of the hessian in deep neural networks. *arXiv preprint arXiv:1902.02366*, 2019.
- Arbel, Michael, A. G. W. L. and Montufar., G. Kernelized wasserstein natural gradient. In *International Conference on Learning Representations*, 2020.
- Bellman, R. The theory of dynamic programming. Technical report, Rand corp santa monica ca, 1954.
- Bertsekas, D. P., Bertsekas, D. P., Bertsekas, D. P., and Bertsekas, D. P. *Dynamic programming and optimal control*, volume 1. Athena scientific Belmont, MA, 1995.
- Boltyanskii, V. G., Gamkrelidze, R. V., and Pontryagin, L. S. The theory of optimal processes. i. the maximum principle. Technical report, TRW SPACE TECHNOLOGY LABS LOS ANGELES CALIF, 1960.
- Chen, T. Q., Rubanova, Y., Bettencourt, J., and Duvenaud, D. K. Neural ordinary differential equations. In *Advances in Neural Information Processing Systems*, pp. 6572–6583, 2018.
- Chung, J., Gulcehre, C., Cho, K., and Bengio, Y. Gated feedback recurrent neural networks. In *International conference on machine learning*, pp. 2067–2075, 2015.
- DE O. PANTOJA, J. Differential dynamic programming and newton’s method. *International Journal of Control*, 47(5):1539–1553, 1988.
- George, T., Laurent, C., Bouthillier, X., Ballas, N., and Vincent, P. Fast approximate natural gradient descent in a kronecker factored eigenbasis. In *Advances in Neural Information Processing Systems*, pp. 9550–9560, 2018.
- Greydanus, S., Dzamba, M., and Yosinski, J. Hamiltonian neural networks. In *Advances in Neural Information Processing Systems*, pp. 15353–15363, 2019.
- Hinton, G., Srivastava, N., and Swersky, K. Neural networks for machine learning lecture 6a overview of mini-batch gradient descent. 2012.
- Hu, B. and Lessard, L. Control interpretations for first-order optimization methods. In *2017 American Control Conference (ACC)*, pp. 3114–3119. IEEE, 2017.
- Huh, M., Sun, S.-H., and Zhang, N. Feedback adversarial learning: Spatial feedback for improving generative adversarial networks. In *Proceedings of the IEEE Conference on Computer Vision and Pattern Recognition*, pp. 1476–1485, 2019.
- Jacobson, D. H. and Mayne, D. Q. Differential dynamic programming. 1970.

- Li, Q. and Hao, S. An optimal control approach to deep learning and applications to discrete-weight neural networks. *arXiv preprint arXiv:1803.01299*, 2018.
- Li, Q., Chen, L., Tai, C., and Weinan, E. Maximum principle based algorithms for deep learning. *The Journal of Machine Learning Research*, 18(1):5998–6026, 2017.
- Li, Z., Yang, J., Liu, Z., Yang, X., Jeon, G., and Wu, W. Feedback network for image super-resolution. In *Proceedings of the IEEE Conference on Computer Vision and Pattern Recognition*, pp. 3867–3876, 2019.
- Liao, L.-Z. and Shoemaker, C. A. Convergence in unconstrained discrete-time differential dynamic programming. *IEEE Transactions on Automatic Control*, 36(6):692–706, 1991.
- Liao, L.-z. and Shoemaker, C. A. Advantages of differential dynamic programming over newton’s method for discrete-time optimal control problems. Technical report, Cornell University, 1992.
- Liu, G.-H. and Theodorou, E. A. Deep learning theory review: An optimal control and dynamical systems perspective. *arXiv preprint arXiv:1908.10920*, 2019.
- Liu, X., Xiao, T., Si, S., Cao, Q., Kumar, S., and Hsieh, C.-J. Neural sde: Stabilizing neural ode networks with stochastic noise. *arXiv preprint arXiv:1906.02355*, 2019.
- Long, Z., Lu, Y., Ma, X., and Dong, B. Pde-net: Learning pdes from data. *arXiv preprint arXiv:1710.09668*, 2017.
- Lu, Y., Zhong, A., Li, Q., and Dong, B. Beyond finite layer neural networks: Bridging deep architectures and numerical differential equations. *arXiv preprint arXiv:1710.10121*, 2017.
- Lu, Y., Li, Z., He, D., Sun, Z., Dong, B., Qin, T., Wang, L., and Liu, T.-Y. Understanding and improving transformer from a multi-particle dynamic system point of view. *arXiv preprint arXiv:1906.02762*, 2019.
- Martens, J. and Grosse, R. Optimizing neural networks with kronecker-factored approximate curvature. In *International conference on machine learning*, pp. 2408–2417, 2015.
- Mayne, D. Q. Differential dynamic programming—a unified approach to the optimization of dynamic systems. In *Control and Dynamic Systems*, volume 10, pp. 179–254. Elsevier, 1973.
- Posa, M., Kuindersma, S., and Tedrake, R. Optimization and stabilization of trajectories for constrained dynamical systems. In *2016 IEEE International Conference on Robotics and Automation (ICRA)*, pp. 1366–1373. IEEE, 2016.
- Seidman, J. H., Fazlyab, M., Preciado, V. M., and Pappas, G. J. Robust deep learning as optimal control: Insights and convergence guarantees. *Proceedings of Machine Learning Research vol xxx*, 1:14, 2020.
- Shama, F., Mechrez, R., Shoshan, A., and Zelnik-Manor, L. Adversarial feedback loop. In *Proceedings of the IEEE International Conference on Computer Vision*, pp. 3205–3214, 2019.
- Tassa, Y., Erez, T., and Todorov, E. Synthesis and stabilization of complex behaviors through online trajectory optimization. In *2012 IEEE/RSJ International Conference on Intelligent Robots and Systems*, pp. 4906–4913. IEEE, 2012.
- Tassa, Y., Mansard, N., and Todorov, E. Control-limited differential dynamic programming. In *2014 IEEE International Conference on Robotics and Automation (ICRA)*, pp. 1168–1175. IEEE, 2014.
- Todorov, E. Optimal control theory. *Bayesian brain: probabilistic approaches to neural coding*, pp. 269–298, 2016.
- Todorov, E. and Li, W. A generalized iterative lqg method for locally-optimal feedback control of constrained nonlinear stochastic systems. In *Proceedings of the 2005, American Control Conference, 2005.*, pp. 300–306. IEEE, 2005.
- Vaswani, S., Mishkin, A., Laradji, I., Schmidt, M., Gidel, G., and Lacoste-Julien, S. Painless stochastic gradient: Interpolation, line-search, and convergence rates. In *Advances in Neural Information Processing Systems*, pp. 3727–3740, 2019.
- Weinan, E. A proposal on machine learning via dynamical systems. *Communications in Mathematics and Statistics*, 5(1):1–11, 2017.
- Weinan, E., Han, J., and Li, Q. A mean-field optimal control formulation of deep learning. *arXiv preprint arXiv:1807.01083*, 2018.
- Wen, H., Han, K., Shi, J., Zhang, Y., Culurciello, E., and Liu, Z. Deep predictive coding network for object recognition. *arXiv preprint arXiv:1802.04762*, 2018.
- Zamir, A. R., Wu, T.-L., Sun, L., Shen, W. B., Shi, B. E., Malik, J., and Savarese, S. Feedback networks. In *Proceedings of the IEEE Conference on Computer Vision and Pattern Recognition*, pp. 1308–1317, 2017.
- Zhong, Y. D., Dey, B., and Chakraborty, A. Symplectic ode-net: Learning hamiltonian dynamics with control. *arXiv preprint arXiv:1909.12077*, 2019.

Supplementary Material

A. Derivation of Batch PMP

A.1. Problem Formulation and Notation

Recall the original OCP for single trajectory optimization. In its batch setting, we consider the following state-augmented optimal control problem:

$$\min_{\bar{\mathbf{u}}} \mathbf{J}(\bar{\mathbf{u}}; \mathbf{X}_0) := \left[\Phi(\mathbf{X}_T) + \sum_{t=0}^{T-1} \mathbf{L}_t(\mathbf{X}_t, \mathbf{u}_t) \right], \quad \text{s.t. } \mathbf{X}_{t+1} = \mathbf{F}_t(\mathbf{X}_t, \mathbf{u}_t), \quad (17)$$

where $\mathbf{X}_t \triangleq [\dots \mathbf{x}_t^{(i)\top} \dots]^\top \in \mathbb{R}^{Bn_t}$ denotes the state-augmented vector over each $\mathbf{x}_t^{(i)} \in \mathbb{R}^{n_t}$, $\forall i \in \{1, 2, \dots, B\}$, and B denotes the batch size. $\mathbf{L}_t(\mathbf{X}_t, \mathbf{u}_t)$ and $\Phi(\mathbf{X}_T)$ respectively represent the average intermediate and terminal cost over $\ell_t(\mathbf{x}_t^{(i)}, \mathbf{u}_t)$ and $\phi(\mathbf{x}_T^{(i)})$. \mathbf{F}_t consists of B independent mappings from each dynamics $f_t(\mathbf{x}_t^{(i)}, \cdot)$. Consequently, its derivatives can be related to the ones for each sample by

$$\begin{aligned} \nabla_{\mathbf{u}_t} \mathbf{F}_t(\mathbf{X}_t, \mathbf{u}_t) &\equiv \mathbf{F}_{\mathbf{u}}^t \in \mathbb{R}^{Bn_{t'} \times m_t}, & \text{where } [\mathbf{F}_{\mathbf{u}}^t]_{(Bn_{t'}, :)} &= f_{\mathbf{u}}^t|^{(i)} \\ \nabla_{\mathbf{X}_t} \mathbf{F}_t(\mathbf{X}_t, \mathbf{u}_t) &\equiv \mathbf{F}_{\mathbf{X}}^t \in \mathbb{R}^{Bn_{t'} \times Bn_t}, & \text{where } [\mathbf{F}_{\mathbf{X}}^t]_{(Bn_{t'}, Bn_t^{(j)})} &= \delta_{ij} f_{\mathbf{x}}^t|^{(i)}, \\ \nabla_{\mathbf{u}_t \mathbf{X}_t} \mathbf{F}_t(\mathbf{X}_t, \mathbf{u}_t) &\equiv \mathbf{F}_{\mathbf{uX}}^t \in \mathbb{R}^{Bn_{t'} \times m_t \times Bn_t}, & \text{where } [\mathbf{F}_{\mathbf{uX}}^t]_{(Bn_{t'}, :, Bn_t^{(j)})} &= \delta_{ij} f_{\mathbf{uX}}^t|^{(i)}, \\ \nabla_{\mathbf{X}_t \mathbf{X}_t} \mathbf{F}_t(\mathbf{X}_t, \mathbf{u}_t) &\equiv \mathbf{F}_{\mathbf{XX}}^t \in \mathbb{R}^{Bn_{t'} \times Bn_t \times Bn_t}, & \text{where } [\mathbf{F}_{\mathbf{XX}}^t]_{(Bn_{t'}, Bn_t^{(j)}, Bn_t^{(k)})} &= \delta_{ijk} f_{\mathbf{XX}}^t|^{(i)}, \\ \nabla_{\mathbf{u}_t \mathbf{u}_t} \mathbf{F}_t(\mathbf{X}_t, \mathbf{u}_t) &\equiv \mathbf{F}_{\mathbf{uu}}^t \in \mathbb{R}^{Bn_{t'} \times m_t \times m_t}, & \text{where } [\mathbf{F}_{\mathbf{uu}}^t]_{(Bn_{t'}, :, :)} &= f_{\mathbf{uu}}^t|^{(i)}. \end{aligned} \quad (18)$$

δ_{ij} and δ_{ijk} represent the Kronecker delta. For simplicity, we denote $t' \triangleq t + 1$, $B_d^{(i)} \triangleq ((i-1)d : id)$ as the indices for i -th block, each with the dimension d , and $f_{\mathbf{uX}}^t|^{(i)} \triangleq \nabla_{\mathbf{u}_t \mathbf{x}_t} f_t(\mathbf{x}_t^{(i)}, \mathbf{u}_t)$ as the derivative of the dynamics of the sample i . Notice again that t appears in the subscript of the gradient since we allow changing the dimension of \mathbf{X}_t at each layer.

A.2. Formal Statement for Proposition 4

Proposition 6. *Let $\bar{\mathbf{u}}^*$ be the optimal control trajectory for the augmented problem described in Eq. (17) and $\bar{\mathbf{X}}^*$ be the corresponding augmented state trajectory. Then, there exists a co-state trajectory $\bar{\mathbf{P}}^* \triangleq \{\mathbf{P}_t^*\}_{t=1}^T$, such that the following 'augmented' PMP equations are satisfied:*

$$\mathbf{X}_{t+1}^* = \nabla_{\mathbf{P}_{t+1}} \mathbf{H}(\mathbf{X}_t^*, \mathbf{P}_{t+1}^*, \mathbf{u}_t^*), \quad \mathbf{X}_0^* = \mathbf{X}_0, \quad (19a)$$

$$\mathbf{P}_t^* = \nabla_{\mathbf{X}_t} \mathbf{H}(\mathbf{X}_t^*, \mathbf{P}_{t+1}^*, \mathbf{u}_t^*), \quad \mathbf{P}_T^* = \nabla_{\mathbf{X}_T} \Phi(\mathbf{X}_T^*), \quad (19b)$$

$$\mathbf{u}_t^* = \arg \min_{\mathbf{v}} \mathbf{H}(\mathbf{X}_t^*, \mathbf{P}_{t+1}^*, \mathbf{v}), \quad \forall \mathbf{v} \in \mathbb{R}^{m_t}, \quad (19c)$$

where the augmented Hamiltonian $\mathbf{H} : \mathbb{R}^{Bn_t} \times \mathbb{R}^{Bn_{t+1}} \times \mathbb{R}^{m_t} \mapsto \mathbb{R}$ at each time step is given by

$$\mathbf{H}(\mathbf{X}_t, \mathbf{P}_{t+1}, \mathbf{u}_t) = \mathbf{P}_{t+1}^\top \mathbf{F}_t(\mathbf{X}_t, \mathbf{u}_t) + \mathbf{L}_t(\mathbf{X}_t, \mathbf{u}_t). \quad (20)$$

Furthermore, solving Eq. (19c) iteratively by $\mathbf{u}_t^{(k+1)} = \mathbf{u}_t^{(k)} - \eta \nabla_{\mathbf{u}_t} \mathbf{H}(\mathbf{X}_t, \mathbf{P}_{t+1}, \mathbf{u}_t^{(k)})$ is equivalent to applying mini-batch gradient descent with Back-propagation.

Proof. It is obvious to see that Eq. (19a) forward propagates each $\mathbf{x}_t^{(i)}$. To bridge Eq. (19b) to the mini-batch Back-propagation, we first notice that the augmented co-state at the terminal time admits a simple form:

$$\mathbf{P}_T = \nabla_{\mathbf{X}_T} \Phi(\mathbf{X}_T) = \frac{1}{B} \begin{bmatrix} \nabla_{\mathbf{x}_T} \phi(\mathbf{x}_T^{(1)}) \\ \vdots \\ \nabla_{\mathbf{x}_T} \phi(\mathbf{x}_T^{(B)}) \end{bmatrix} = \frac{1}{B} \begin{bmatrix} \mathbf{p}_T^{(1)} \\ \vdots \\ \mathbf{p}_T^{(B)} \end{bmatrix}. \quad (21)$$

In other words, \mathbf{P}_T is a collection over each co-state $\mathbf{p}_T^{(i)}$ and normalizes by the batch size. We can show by induction that such a structure is preserved throughout the adjoint dynamics in Eq. (19b):

$$\begin{aligned} \mathbf{P}_t &= \nabla_{\mathbf{X}_t} \mathbf{H}(\mathbf{X}_t, \mathbf{P}_{t+1}, \mathbf{u}_t) \\ &= \mathbf{L}_{\mathbf{X}}^t + \mathbf{F}_{\mathbf{X}}^t \mathbf{P}_{t+1} \\ &= \frac{1}{B} \begin{bmatrix} \nabla_{\mathbf{x}_t} \ell_t(\mathbf{x}_t^{(1)}, \mathbf{u}_t) + \nabla_{\mathbf{x}_t} f_t(\mathbf{x}_t^{(1)}, \mathbf{u}_t)^\top \mathbf{p}_{t+1}^{(1)} \\ \vdots \\ \nabla_{\mathbf{x}_t} \ell_t(\mathbf{x}_t^{(B)}, \mathbf{u}_t) + \nabla_{\mathbf{x}_t} f_t(\mathbf{x}_t^{(B)}, \mathbf{u}_t)^\top \mathbf{p}_{t+1}^{(B)} \end{bmatrix} = \frac{1}{B} \begin{bmatrix} \mathbf{p}_t^{(1)} \\ \vdots \\ \mathbf{p}_t^{(B)} \end{bmatrix}. \end{aligned} \quad (22)$$

Finally, the update direction is given by

$$\begin{aligned} \nabla_{\mathbf{u}_t} \mathbf{H}(\mathbf{X}_t, \mathbf{P}_{t+1}, \mathbf{u}_t) &= \mathbf{L}_{\mathbf{u}}^t + \mathbf{F}_{\mathbf{u}}^t \mathbf{P}_{t+1} \\ &= \frac{1}{B} \sum_i \nabla_{\mathbf{u}_t} \ell_t(\mathbf{x}_t^{(i)}, \mathbf{u}_t) + \frac{1}{B} \sum_i [\mathbf{F}_{\mathbf{u}}^t]_{(B^{n_{t+1}}, \cdot)}^\top \mathbf{p}_{t+1}^{(i)} \\ &= \frac{1}{B} \sum_i \nabla_{\mathbf{u}_t} \ell_t(\mathbf{x}_t^{(i)}, \mathbf{u}_t) + \nabla_{\mathbf{u}_t} f_t(\mathbf{x}_t^{(i)}, \mathbf{u}_t)^\top \mathbf{p}_{t+1}^{(i)} \\ &= \frac{1}{B} \sum_i \nabla_{\mathbf{u}_t} H(\mathbf{x}_t^{(i)}, \mathbf{u}_t, \mathbf{p}_{t+1}^{(i)}) = \frac{1}{B} \sum_i \nabla_{\mathbf{u}_t} J(\mathbf{u}_t; \mathbf{x}_0^{(i)}), \end{aligned} \quad (23)$$

which is the exact mini-batch gradient update. \square

Remarks: It should be stressed that the relation between \mathbf{P}_t and \mathbf{p}_t by simply taking the average is only true when first-order derivatives are involved. In Appendix B.2, we will show that the backward pass for the augmented value function does not admit this property and therefore can be much complex.

B. Derivation of Batch DDP for Feedforward Networks

In this part we provide the complete derivation in Sec. 4 for optimizing feedforward networks with batch DDP optimizer.

B.1. Feedforward Networks as Dynamical Systems

We first consider the original DDP formulation when feedforward networks are used as dynamics. Here we provide derivations for the new δQ expansion (i.e. Eq. (13)) and how it can be computed efficiently (i.e. Eq. (14)).

Derivation of Eq. (13). It is sufficient to derive $Q_{\mathbf{u}}$ and $Q_{\mathbf{u}\mathbf{u}}$ only, which are given respectively by

$$\begin{aligned} Q_{\mathbf{u}} &= \ell_{\mathbf{u}} + f_{\mathbf{u}}^\top V'_{\mathbf{x}'} = \ell_{\mathbf{u}} + g_{\mathbf{u}}^\top \sigma_{\mathbf{h}}^\top V'_{\mathbf{x}'}, \quad (24) \\ Q_{\mathbf{u}\mathbf{u}} &= \ell_{\mathbf{u}\mathbf{u}} + \frac{\partial}{\partial \mathbf{u}} \{g_{\mathbf{u}}^\top \sigma_{\mathbf{h}}^\top V'_{\mathbf{x}'}\} \\ &= \ell_{\mathbf{u}\mathbf{u}} + g_{\mathbf{u}}^\top \sigma_{\mathbf{h}}^\top \frac{\partial}{\partial \mathbf{u}} \{V'_{\mathbf{x}'}\} + g_{\mathbf{u}}^\top \left(\frac{\partial}{\partial \mathbf{u}} \{\sigma_{\mathbf{h}}\} \right)^\top V'_{\mathbf{x}'} + \left(\frac{\partial}{\partial \mathbf{u}} \{g_{\mathbf{u}}\} \right)^\top \sigma_{\mathbf{h}}^\top V'_{\mathbf{x}'} \\ &= \ell_{\mathbf{u}\mathbf{u}} + g_{\mathbf{u}}^\top \sigma_{\mathbf{h}}^\top V'_{\mathbf{x}'\mathbf{x}'} \sigma_{\mathbf{h}} g_{\mathbf{u}} + g_{\mathbf{u}}^\top (V'_{\mathbf{x}'}^\top \sigma_{\mathbf{h}\mathbf{h}} g_{\mathbf{u}}) + g_{\mathbf{u}\mathbf{u}}^\top \sigma_{\mathbf{h}}^\top V'_{\mathbf{x}'} \\ &= \ell_{\mathbf{u}\mathbf{u}} + g_{\mathbf{u}}^\top (V_{\mathbf{h}\mathbf{h}} + V'_{\mathbf{x}'} \cdot \sigma_{\mathbf{h}\mathbf{h}}) g_{\mathbf{u}} + V_{\mathbf{h}} \cdot g_{\mathbf{u}\mathbf{u}} \end{aligned} \quad (25)$$

The last equation follows by recalling $V_{\mathbf{h}} \triangleq \sigma_{\mathbf{h}}^\top V'_{\mathbf{x}'}$ and $V_{\mathbf{h}\mathbf{h}} \triangleq \sigma_{\mathbf{h}}^\top V'_{\mathbf{x}'\mathbf{x}'} \sigma_{\mathbf{h}}$.

Derivation of Eq. (14). First, recall the affine transform $g_t = \mathbf{W}_t \mathbf{x}_t + \mathbf{b}_t$, where $\mathbf{W}_t \in \mathbb{R}^{n_{t+1} \times n_t}$, and $\mathbf{b}_t \in \mathbb{R}^{n_{t+1}}$. The i -th element of the vector g_t can be written as

$$[g]_i = \sum_{k=1}^{n_t} [\mathbf{W}]_{(i,k)} [\mathbf{x}]_k + [\mathbf{b}]_i = \sum_{k=1}^{n_t} [\mathbf{u}]_{(k-1)n_{t+1}+i} [\mathbf{x}]_k + [\mathbf{u}]_{n_t n_{t+1}+i}, \quad (26)$$

where we omit the subscript t for simplicity and introduce the vectorized variable $\mathbf{u} = [\text{vec}(\mathbf{W}), \mathbf{b}]^\top$. It can be readily verified that

$$[g_{\mathbf{u}\mathbf{x}}]_{(i,j,k)} = 1 \quad \text{iff} \quad j = (k-1)n_{t+1} + i, \quad \forall k \in \{1, \dots, n_t\}. \quad (27)$$

Thus, $g_{\mathbf{u}\mathbf{x}}$ is a sparse tensor with each block $[g_{\mathbf{u}\mathbf{x}}]_{(:,B_{n_{t+1}}^{(k)},k)}$ being an identity matrix $\mathbf{I}_{n_{t+1}}$, and its tensor operation can be computed by

$$[\mathbf{V}_h \cdot g_{\mathbf{u}\mathbf{x}}]_{(j,k)} = \sum_{i=1}^{n_{t+1}} [g_{\mathbf{u}\mathbf{x}}]_{(i,j,k)} [\mathbf{V}_h]_i = [\mathbf{V}_h]_{j-(k-1)n_{t+1}}, \quad \forall k \in \{1, \dots, n_t\}. \quad (28)$$

In other words, $\mathbf{V}_h \cdot g_{\mathbf{u}\mathbf{x}}$ consists of n_t vectors \mathbf{V}_h , with the indices given by Eq. (14).

B.2. Batch DDP Formulation

Next, we extend the formulation in Appendix B.1 to the batch setting by adopting the same notation in Appendix A.1. Given the augmented Bellman objective $\mathbf{Q}(\mathbf{X}_t, \mathbf{u}_t) \triangleq \mathbf{L}_t(\mathbf{X}_t, \mathbf{u}_t) + \mathbf{V}_{t+1}(\mathbf{F}_t(\mathbf{X}_t, \mathbf{u}_t))$, we modify Eq. (13) by substituting $\mathbf{F}_t \equiv \sigma_t \circ \mathbf{G}_t$,

$$\mathbf{Q}_{\mathbf{X}}^t = \mathbf{L}_{\mathbf{X}}^t + \mathbf{F}_{\mathbf{X}}^{t\top} \mathbf{V}'_{\mathbf{X}'} = \mathbf{L}_{\mathbf{X}}^t + \mathbf{G}_{\mathbf{X}}^{t\top} \mathbf{V}_{\mathbf{H}}^t \quad (29a)$$

$$\mathbf{Q}_{\mathbf{u}}^t = \mathbf{L}_{\mathbf{u}}^t + \mathbf{F}_{\mathbf{u}}^{t\top} \mathbf{V}'_{\mathbf{X}'} = \mathbf{L}_{\mathbf{u}}^t + \mathbf{G}_{\mathbf{u}}^{t\top} \mathbf{V}_{\mathbf{H}}^t \quad (29b)$$

$$\begin{aligned} \mathbf{Q}_{\mathbf{X}\mathbf{X}}^t &= \mathbf{L}_{\mathbf{X}\mathbf{X}}^t + \mathbf{F}_{\mathbf{X}}^{t\top} \mathbf{V}'_{\mathbf{X}'\mathbf{X}'} \mathbf{F}_{\mathbf{X}}^t + \mathbf{V}'_{\mathbf{X}'} \cdot \mathbf{F}_{\mathbf{X}\mathbf{X}}^t \\ &= \mathbf{L}_{\mathbf{X}\mathbf{X}}^t + \mathbf{G}_{\mathbf{X}}^{t\top} (\mathbf{V}_{\mathbf{H}\mathbf{H}}^t + \mathbf{V}'_{\mathbf{X}'} \cdot \sigma_{\mathbf{H}\mathbf{H}}^t) \mathbf{G}_{\mathbf{X}}^t + \mathbf{V}_{\mathbf{H}}^t \cdot \mathbf{G}_{\mathbf{X}\mathbf{X}}^t \end{aligned} \quad (29c)$$

$$\begin{aligned} \mathbf{Q}_{\mathbf{u}\mathbf{u}}^t &= \mathbf{L}_{\mathbf{u}\mathbf{u}}^t + \mathbf{F}_{\mathbf{u}}^{t\top} \mathbf{V}'_{\mathbf{X}'\mathbf{X}'} \mathbf{F}_{\mathbf{u}}^t + \mathbf{V}'_{\mathbf{X}'} \cdot \mathbf{F}_{\mathbf{u}\mathbf{u}}^t \\ &= \mathbf{L}_{\mathbf{u}\mathbf{u}}^t + \mathbf{G}_{\mathbf{u}}^{t\top} (\mathbf{V}_{\mathbf{H}\mathbf{H}}^t + \mathbf{V}'_{\mathbf{X}'} \cdot \sigma_{\mathbf{H}\mathbf{H}}^t) \mathbf{G}_{\mathbf{u}}^t + \mathbf{V}_{\mathbf{H}}^t \cdot \mathbf{G}_{\mathbf{u}\mathbf{u}}^t \end{aligned} \quad (29d)$$

$$\begin{aligned} \mathbf{Q}_{\mathbf{u}\mathbf{X}}^t &= \mathbf{L}_{\mathbf{u}\mathbf{X}}^t + \mathbf{F}_{\mathbf{u}}^{t\top} \mathbf{V}'_{\mathbf{X}'\mathbf{X}'} \mathbf{F}_{\mathbf{X}}^t + \mathbf{V}'_{\mathbf{X}'} \cdot \mathbf{F}_{\mathbf{u}\mathbf{X}}^t \\ &= \mathbf{L}_{\mathbf{u}\mathbf{X}}^t + \mathbf{G}_{\mathbf{u}}^{t\top} (\mathbf{V}_{\mathbf{H}\mathbf{H}}^t + \mathbf{V}'_{\mathbf{X}'} \cdot \sigma_{\mathbf{H}\mathbf{H}}^t) \mathbf{G}_{\mathbf{X}}^t + \mathbf{V}_{\mathbf{H}}^t \cdot \mathbf{G}_{\mathbf{u}\mathbf{X}}^t, \end{aligned} \quad (29e)$$

where $\mathbf{V}_{\mathbf{H}}^t$ and $\mathbf{V}_{\mathbf{H}\mathbf{H}}^t$ are given by

$$\mathbf{V}_{\mathbf{H}}^t \triangleq \sigma_{\mathbf{H}}^{t\top} \mathbf{V}'_{\mathbf{X}'}, \quad \mathbf{V}_{\mathbf{H}\mathbf{H}}^t \triangleq \sigma_{\mathbf{H}}^{t\top} \mathbf{V}'_{\mathbf{X}'\mathbf{X}'} \sigma_{\mathbf{H}}^t. \quad (30)$$

Once we have all the \mathbf{Q} derivatives explicitly written, computing layer-wise feedback policies and backward passing the derivatives of the augmented value follow by the same equations as in the original DDP, i.e.

$$\delta \mathbf{u}_t^* (\delta \mathbf{X}_t) = \bar{\mathbf{k}}_t + \bar{\mathbf{K}}_t \delta \mathbf{X}_t = -(\mathbf{Q}_{\mathbf{u}\mathbf{u}}^t)^{-1} (\mathbf{Q}_{\mathbf{u}}^t + \mathbf{Q}_{\mathbf{u}\mathbf{X}}^t \delta \mathbf{X}_t), \quad (31)$$

$$\begin{aligned} \mathbf{V}_{\mathbf{X}}^t &= \mathbf{Q}_{\mathbf{X}}^t - \mathbf{Q}_{\mathbf{u}\mathbf{X}}^{t\top} (\mathbf{Q}_{\mathbf{u}\mathbf{u}}^t)^{-1} \mathbf{Q}_{\mathbf{u}}^t = \mathbf{Q}_{\mathbf{X}}^t + \mathbf{Q}_{\mathbf{u}\mathbf{X}}^{t\top} \bar{\mathbf{k}}_t, \\ \mathbf{V}_{\mathbf{X}\mathbf{X}}^t &= \mathbf{Q}_{\mathbf{X}\mathbf{X}}^t - \mathbf{Q}_{\mathbf{u}\mathbf{X}}^{t\top} (\mathbf{Q}_{\mathbf{u}\mathbf{u}}^t)^{-1} \mathbf{Q}_{\mathbf{u}\mathbf{X}}^t = \mathbf{Q}_{\mathbf{X}\mathbf{X}}^t + \mathbf{Q}_{\mathbf{u}\mathbf{X}}^{t\top} \bar{\mathbf{K}}_t. \end{aligned} \quad (32)$$

To see whether the backward pass of the augmented value function inherits any implicit structure, similar to the average relation in Eq. (22). Let us rewrite Eq. (29) in a block-wise fashion by recalling Eq. (18).

$$\mathbf{Q}_{\mathbf{u}}^t = \frac{1}{B} \sum_i \ell_{\mathbf{u}}^t |^{(i)} + \sum_i f_{\mathbf{u}}^t |^{(i)\top} [\mathbf{V}'_{\mathbf{X}'}]_{B_{n_t}^{(i)}} \quad (33a)$$

$$[\mathbf{Q}_{\mathbf{X}}^t]_{B_{n_t}^{(i)}} = \frac{1}{B} \ell_{\mathbf{x}}^t |^{(i)} + f_{\mathbf{x}}^t |^{(i)\top} [\mathbf{V}'_{\mathbf{X}'}]_{B_{n_t}^{(i)}} \quad (33b)$$

$$[\mathbf{Q}_{\mathbf{u}\mathbf{X}}^t]_{(:,B_{n_t}^{(i)})} = \frac{1}{B} \ell_{\mathbf{u}\mathbf{x}}^t |^{(i)} + \sum_j f_{\mathbf{u}}^t |^{(j)\top} [\mathbf{V}'_{\mathbf{X}'\mathbf{X}'}]_{(B_{n_t}^{(j)}, B_{n_t}^{(i)})} f_{\mathbf{x}}^t |^{(j)} + [\mathbf{V}'_{\mathbf{X}'}]_{B_{n_t}^{(i)}} \cdot f_{\mathbf{u}\mathbf{x}}^t |^{(i)} \quad (33c)$$

$$[\mathbf{Q}_{\mathbf{X}\mathbf{X}}^t]_{(B_{n_t}^{(i)}, B_{n_t}^{(j)})} = \frac{1}{B} \delta_{ij} \ell_{\mathbf{x}(\mathbf{x})}^t |^{(i)} + f_{\mathbf{x}}^t |^{(i)\top} [\mathbf{V}'_{\mathbf{X}'\mathbf{X}'}]_{(B_{n_t}^{(i)}, B_{n_t}^{(j)})} f_{\mathbf{x}}^t |^{(j)} + \delta_{ij} ([\mathbf{V}'_{\mathbf{X}'}]_{B_{n_t}^{(i)}} \cdot f_{\mathbf{x}\mathbf{x}}^t |^{(j)}) \quad (33d)$$

$$\mathbf{Q}_{\mathbf{u}\mathbf{u}}^t = \frac{1}{B} \sum_i \ell_{\mathbf{u}\mathbf{u}}^t |^{(i)} + \sum_{ij} f_{\mathbf{u}}^t |^{(i)\top} [\mathbf{V}'_{\mathbf{X}'\mathbf{X}'}]_{(B_{n_t}^{(i)}, B_{n_t}^{(j)})} f_{\mathbf{u}}^t |^{(j)} + \sum_i [\mathbf{V}'_{\mathbf{X}'}]_{B_{n_t}^{(i)}} \cdot f_{\mathbf{u}\mathbf{u}}^t |^{(i)} \quad (33e)$$

Notice that at $t = T$, the derivatives of the augmented value function are related to the ones for each sample by:

$$[\mathbf{V}_{\mathbf{X}}^T]_{B_{n_T}^{(i)}} = \frac{1}{B} V_{\mathbf{x}^{(i)}}^T, \quad \text{and} \quad [\mathbf{V}_{\mathbf{X}\mathbf{X}}^T]_{(B_{n_T}^{(i)}, B_{n_T}^{(j)})} = \frac{1}{B} \delta_{ij} V_{\mathbf{x}^{(i)}\mathbf{x}^{(j)}}^T. \quad (34)$$

Substitute them into Eq. (33), one can show that the derivatives of the augmented \mathbf{Q} at $t = T - 1$ can indeed be expressed by the composition of each $Q^{(i)}$

$$\begin{aligned} \mathbf{Q}_u^{T-1} &= \frac{1}{B} \sum_i Q_u^{T-1|^{(i)}}, \quad [\mathbf{Q}_X^{T-1}]_{B_{n_t}^{(i)}} = \frac{1}{B} Q_{x^{(i)}}^{T-1}, \\ [\mathbf{Q}_{uX}^{T-1}]_{(:,B_{n_t}^{(i)})} &= \frac{1}{B} Q_{ux^{(i)}}^{T-1}, \quad [\mathbf{Q}_{XX}^{T-1}]_{(B_{n_t}^{(i)},B_{n_t}^{(j)})} = \delta_{ij} \frac{1}{B} Q_{x^{(i)}x^{(j)}}^{T-1}, \quad \mathbf{Q}_{uu}^{T-1} = \frac{1}{B} \sum_i Q_{uu}^{T-1|^{(i)}}. \end{aligned} \quad (35)$$

However, \mathbf{V}_X^{T-1} and \mathbf{V}_{XX}^{T-1} will no longer preserve the structure described in Eq. (34). In fact, we will have

$$[\mathbf{V}_X^{T-1}]_{B_{n_{T-1}}^{(i)}} = \frac{1}{B} \left(Q_{x^{(i)}}^{T-1} - (Q_{ux^{(i)}}^{T-1})^\top (Q_{uu}^{T-1})^{-1} Q_u^{T-1} \right), \text{ and} \quad (36)$$

$$[\mathbf{V}_{XX}^{T-1}]_{(B_{n_{T-1}}^{(i)},B_{n_{T-1}}^{(j)})} = \frac{1}{B} \left(\delta_{ij} Q_{x^{(i)}x^{(j)}}^{T-1} - (Q_{ux^{(i)}}^{T-1})^\top (Q_{uu}^{T-1})^{-1} Q_{ux^{(j)}}^{T-1} \right). \quad (37)$$

Neither \mathbf{V}_X^{T-1} nor \mathbf{V}_{XX}^{T-1} can be expressed by the composition of $V_{x^{(i)}}^{T-1}$ or $V_{x^{(i)}}^{T-1}$. Furthermore, \mathbf{V}_{XX}^{T-1} is no longer a block-diagonal matrix.

C. Others Derivations from the Main Text

C.1. Proof of Proposition 5

First observe the below lemma which connects the backward passes between two frameworks in the degenerate case.

Lemma 7. *Assume $Q_{ux}^t = \mathbf{0}$ at all stages, then we have*

$$\mathbf{V}_x^t = H_x^t = \mathbf{p}_t = \nabla_{x_t} J, \text{ and} \quad \mathbf{V}_{xx}^t = \nabla_{x_t x_t} J, \quad \forall t. \quad (38)$$

Proof. It is obvious to see that Eq. (38) holds at $t = T$. Now, assume the relation holds at $t + 1$ and observe that at the time t , the backward passes take the form of

$$\begin{aligned} \mathbf{p}_t &= H_x^t = \ell_x^t + f_x^{t\top} \mathbf{p}_{t+1} = \nabla_{x_t} J, \\ \mathbf{V}_x^t &= Q_x^t - Q_{ux}^{t\top} (Q_{uu}^t)^{-1} Q_u^t = \ell_x^t + f_x^{t\top} V_x^{t+1}, \\ \mathbf{V}_{xx}^t &= Q_{xx}^t - Q_{ux}^{t\top} (Q_{uu}^t)^{-1} Q_{ux}^t = \nabla_{x_t} \{ \ell_x^t + f_x^{t\top} V_x^{t+1} \} = \nabla_{x_t x_t} J, \end{aligned}$$

which concludes the proof. \square

Now, Eq. (12) follows by substituting Eq. (38) to the definition of Q_u^t and Q_{uu}^t

$$\begin{aligned} Q_u^t &= \ell_u^t + f_u^{t\top} V_x^{t+1} = \ell_u^t + f_u^{t\top} \nabla_{x_{t+1}} J = \nabla_{u_t} J, \\ Q_{uu}^t &= \ell_{uu}^t + f_u^{t\top} V_{xx}^{t+1} f_u^t + V_x^{t+1} \cdot f_{uu}^t \\ &= \ell_{uu}^t + f_u^{t\top} (\nabla_{x_{t'} x_{t'}} J) f_u^t + \nabla_{x_{t'}} J \cdot f_{uu}^t \\ &= \nabla_{u_t} \{ \ell_u^t + f_u^{t\top} \nabla_{x_{t'}} J \} = \nabla_{u_t u_t} J, \end{aligned}$$

where we denote $t' = t + 1$ in the last two equations for simplicity. Consequently, the policy generates to layer-wise Newton update.

C.2. Derivation of Eq. (16)

Eq. (16) follows by a simple observation that the feedback term $\mathbf{K}_t \delta x_t \triangleq -(Q_{uu}^t)^{-1} Q_{ux}^t \delta x_t$ stands as the minimizer of the following objective up to first order approximation:

$$\mathbf{K}_t \delta x_t = \arg \min_{\delta u_t \in \Gamma(\delta x_t)} \|\nabla_{u_t} Q(x_t + \delta x_t, u_t + \delta u_t) - \nabla_{u_t} Q(x_t, u_t)\|, \quad (39)$$

with $\|\cdot\|$ being any proper norm in the Euclidean space. Eq. (39) can be shown by Taylor expanding $Q(x_t + \delta x_t, u_t + \delta u_t)$ up to its first order,

$$\nabla_{u_t} Q(x_t + \delta x_t, u_t + \delta u_t) = \nabla_{u_t} Q(x_t, u_t) + Q_{ux}^t \delta x_t + Q_{uu}^t \delta u_t.$$

When $Q = J$, we will arrive at Eq. (16). While this is generally not true for nontrivial Q_{xu}^t (recall Proposition 5), we shall interpret the Bellman objective Q as the resulting objective when the feedback policies are applied to all the afterward stages, indeed implied in the Bellman equation Eq. (4).

D. Experiment Detail

D.1. Setup

The networks in the classification problems are composed of 5-6 fully-connected layers. For the intermediate layers, we use ReLU activation on (F)MNIST, and Tanh on the other three data set. We use identity mapping at the last prediction layer for all data set except WINE, where we use sigmoid instead to help distinguish the performance among optimizers. The dimension of the hidden state is set to 10 for small data set, such as WINE and IRIS, and 20-32 for other larger data set. The batch size is set to 8 for DIGITS, 16 for (F)MNIST, and 32 for WINE and IRIS. Results reported in all plots and figures are averaged over multiple random seeds (3 seeds for (F)MNIST, and 6-10 for the rest). To accelerate training, we only utilize 50% of the samples in MNIST and FMNIST. Regarding the machine information, we conduct our experiments on GTX 1080 TI, RTX TITAN, and four Tesla V100 SXM2 16GB. For the baseline optimizers, we use the implementation in <https://github.com/Thrandis/EKFAC-pytorch> for KFAC and EKFAC, and <https://github.com/MichaelArbel/KWNG> for KWNG.

D.2. Additional Experiments

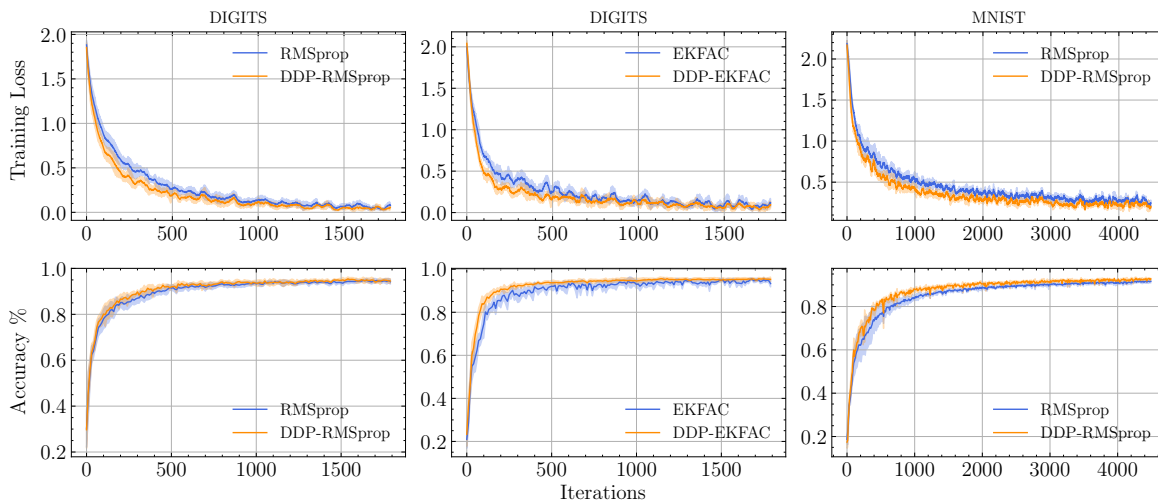


Figure 7. Optimization dynamics of both training loss (upper row) and testing accuracy (bottom row) for the experiment instances in Table 4 with large variance reduction. In all cases, optimizers integrated with DDP also admit slightly faster convergence.

Ablation Analysis on Other Data Set. In Fig. 8, we provide additional results for the ablation analysis on other data set. Similar to the discussion in Fig. 5, DDP effectively suppresses the potentially unstable training due to the change of hyper-parameter. On IRIS data set, notably, optimizers embedded with DDP often lead to much lower training loss in the end.

Remarks on Hyper-parameter Tuning. Recall that in order to stabilize the training, we add Tikhonov regularization to both Q_{uu} and V_{xx} matrices. In practice, we find that the regularization imposed on Q_{uu} generally has greater effect on the overall training dynamics. The performance can degrade when Q_{uu} is regulated either insufficiently or too much. On the other hands, effect of V_{xx} regularization on optimization is typically optimizer-dependent. Empirically, we find that regulating V_{xx} properly plays a key role in improving the performance of DDP-RMSprop, while the two rest are less sensitive to this hyper-parameter.

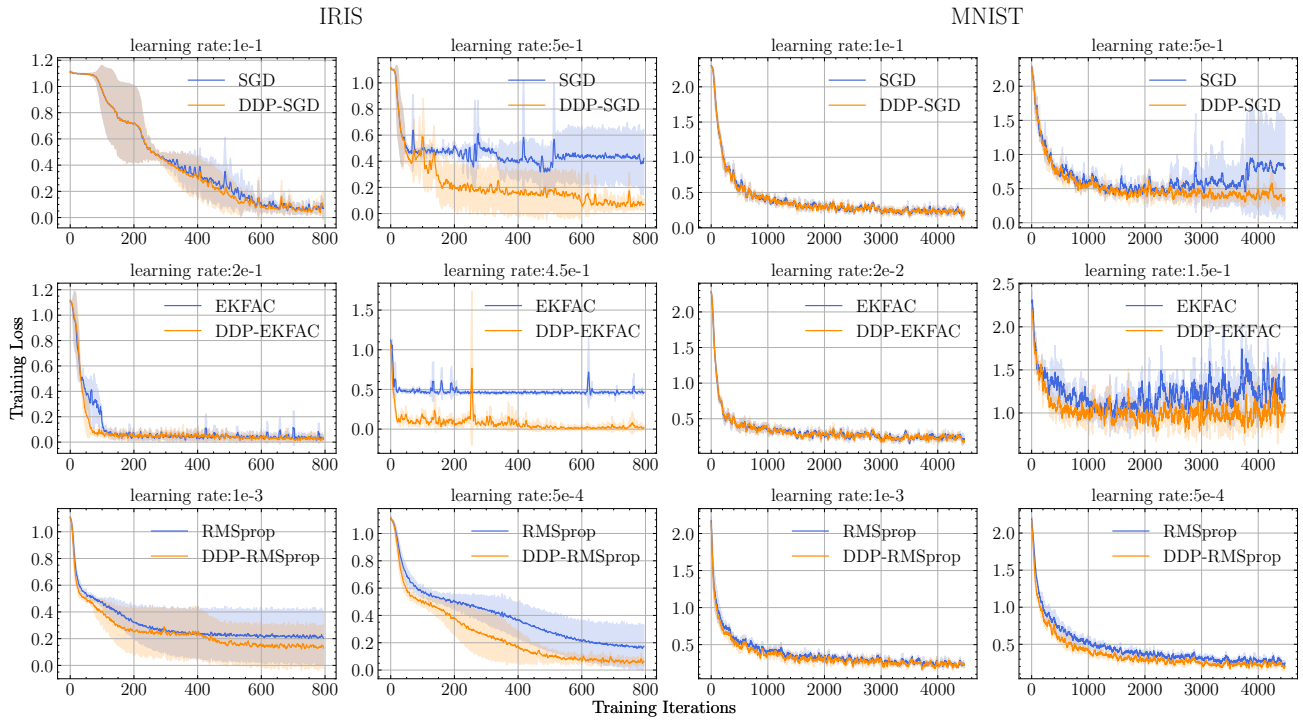


Figure 8. Ablation analysis on other data set. Same as Fig. 5, the first and third columns report the training dynamics on the best-tuned configurations, while the second and last columns correspond to situations where the learning rate gets perturbed.